Article

Density Functional Theory Studies on the Mechanisms of Regioselective Allylic and *cis*-Vinylic Deprotonation of Allyl Amides and Allylamines

Fredrik Haeffner, Madeleine A. Jacobson, Ivan Keresztes, and Paul G. Williard

J. Am. Chem. Soc., **2004**, 126 (51), 17032-17039• DOI: 10.1021/ja0487731 • Publication Date (Web): 02 December 2004

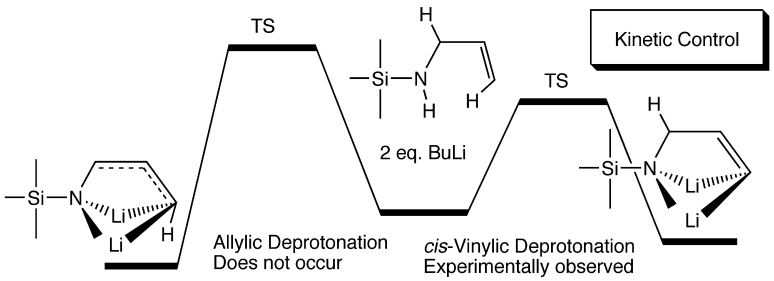

More About This Article

Additional resources and features associated with this article are available within the HTML version:

- Supporting Information
- Access to high resolution figures
- Links to articles and content related to this article
- Copyright permission to reproduce figures and/or text from this article

View the Full Text HTML

J|A|C|S
ARTICLES
Published on Web 12/02/2004

Density Functional Theory Studies on the Mechanisms of Regioselective Allylic and *cis*-Vinylic Deprotonation of Allyl Amides and Allylamines

Fredrik Haeffner,* Madeleine A. Jacobson, Ivan Keresztes, and Paul G. Williard

Contribution from the Department of Chemistry, Brown University, Providence, Rhode Island 02912

Received March 3, 2004; E-mail: fredrick_haeffner@brown.edu

Abstract: A density functional theory (B3LYP/6-31+G*) study was undertaken in an effort to learn more about the mechanisms controlling the regioselective deprotonations of the synthetically versatile *N*-lithio-*N*-(*tert*-butyl)allylamide **1** and *N*-lithio-*N*-(trimethylsilyl)allylamine **2** compounds. The calculations suggest that deprotonation of **1** occurs exclusively at the allylic position. This agrees with experimental results. The calculations also suggest that deprotonation of allylamine **2** exclusively at the *cis*-vinylic position is due to kinetic control.

Introduction

Organolithium compounds have become vital in modern organic synthesis. A detailed molecular understanding of the mechanisms controlling stereo- as well as regioselectivity of these compounds and the reactions they undergo are important for further development of their use in synthetic chemistry.

It has been known for some time that deprotonation of *N*-lithio-*N*-(trimethylsilyl)allylamine **2** occurs exclusively at the *cis*-vinylic position under mild conditions (1 equiv of *n*BuLi, 0 °C, diethyl ether).[1] Alternatively, deprotonation of similar compounds, for example, *N*-lithio-*N*-(*tert*-butyl)allylamide **1** (Figure 1), results in allylic deprotonation under the same conditions.[2,3]

The *cis*-vinyl deprotonation reactions are carried out in ethereal solvents. Surprisingly, no deprotonation reactions occur when THF or diethyl ether is replaced by a hydrocarbon solvent, even at elevated temperatures. However, addition of even small amounts of THF to the hydrocarbon solvent results in deprotonation. On the contrary, no reaction occurred when small amounts of the chelating additive TMEDA were added to the hydrocarbon solution.[3,4]

NMR and X-ray diffraction analysis of the closely related compound 3,*N*-dilithio-*N*-(*tert*-butyldimethylsilyl)allylamine, as well as X-ray diffraction analysis of *N*-dilithio-*N*-(trimethylsilyl)-allylamine **6**, demonstrate that these dianions form a "c-clamp" structure in solution as well as in the solid state.[5,6] In these structures, two lithium ions coordinate on opposite sides of the dianion (Figure 2). The solution structure of 3,*N*-dilithio-*N*-(*tert*-butyldimethylsilyl)allylamine has been investigated and is presented in detail elsewhere.[6]

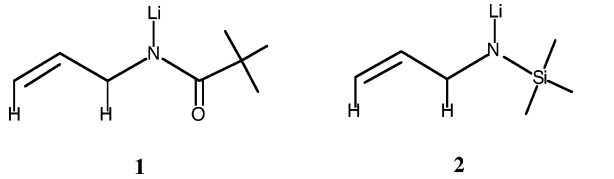

Figure 1. The mechanism controlling the regiospecific deprotonation (*cis*-vinylic versus allylic) of the lithiated allylamide and allylamine compounds **1** and **2** was investigated using density functional theory (B3LYP/6-31+G*).

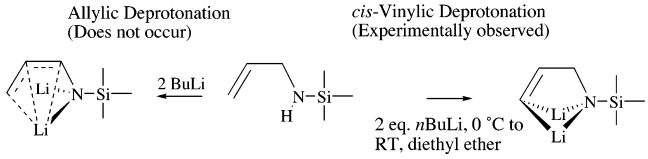

Figure 2. Possible reaction pathways for dilithiation of *N*-(trimethylsilyl)-allylamine.

Semiempirical PM3 geometry optimization of both the experimentally observed c-clamp shaped lithiated vinyl dianion **6** and the unobserved allyl dianion **5** (Figure 3) was performed.[7] Single-point energy calculations using the B3LYP functional and the 6-31+G* basis set were performed on the PM3 optimized geometries.[7] The calculated difference in energy between

(1) Burns, S. A.; Corriu, R. J. P.; Huynh, V.; Moreau, J. J. E. *J. Organomet. Chem.* **1987**, *333*, 281.
(2) For some examples, see: (a) Heinl, T.; Retzow, S.; Hoppe, D.; Fraenkel, G.; Chow, A. *Chem.-Eur. J.* **1999**, *5*, 3464. (b) Ahlbrecht, H.; Schmidt, R.; Beyer, U. *Eur. J. Org. Chem.* **1942**, *7*, 1371. (c) Pippel, D. J.; Weisenburger, G. A.; Wilson, S. R.; Beak, P. *Angew. Chem., Int. Ed.* **1998**, *37*, 2522. (d) Tomooka, K.; Yamamoto, H.; Nakai, T. *Liebigs Ann.* **1997**, *7*, 1275. (e) Park, Y. S.; Weisenburger, G. A.; Beak, P. *J. Am. Chem. Soc.* **1997**, *119*, 10537. (f) Weisenburger, G. A.; Beak, P. *J. Am. Chem. Soc.* **1996**, *118*, 12218. (g) Zschage, O.; Hoppe, D. *Tetrahedron* **1992**, *48*, 8389. (h) Marsch, M.; Harms, K.; Zschage, O.; Hoppe, D.; Boche, G. *Angew. Chem., Int. Ed. Engl.* **1991**, *30*, 321. (i) Hoppe, D. *Nachr. Chem., Tech. Lab.* **1982**, *30*, 483. (j) Neijzen, B. *Chem. Technol.* **1970**, *25*, 393.
(3) Jacobson, M. A., unpublished results.
(4) Jacobson, M. A.; Williard, P. G. *J. Org. Chem.* **2002**, *67*, 32.
(5) Williard, P. G.; Jacobson, M. A. *Org. Lett.* **2000**, *2*, 2753.
(6) Jacobson, M. A.; Keresztes, I.; Williard, P. G., manuscript submitted for publication.
(7) Unpublished results. PM3: Stewart, J. J P. *J. Comput. Chem.* **1989**, *10*, 209. Li parameters: Anders, E.; Koch, R.; Freunscht, P. *J. Comput. Chem.* **1993**, *14*, 1301. The calulations were performed with PC Spartan Pro, Wavefunction Inc., 18401 Von Karman Ave., Suite 370, Irvine, CA 92715.

10.1021/ja0487731 CCC: $27.50

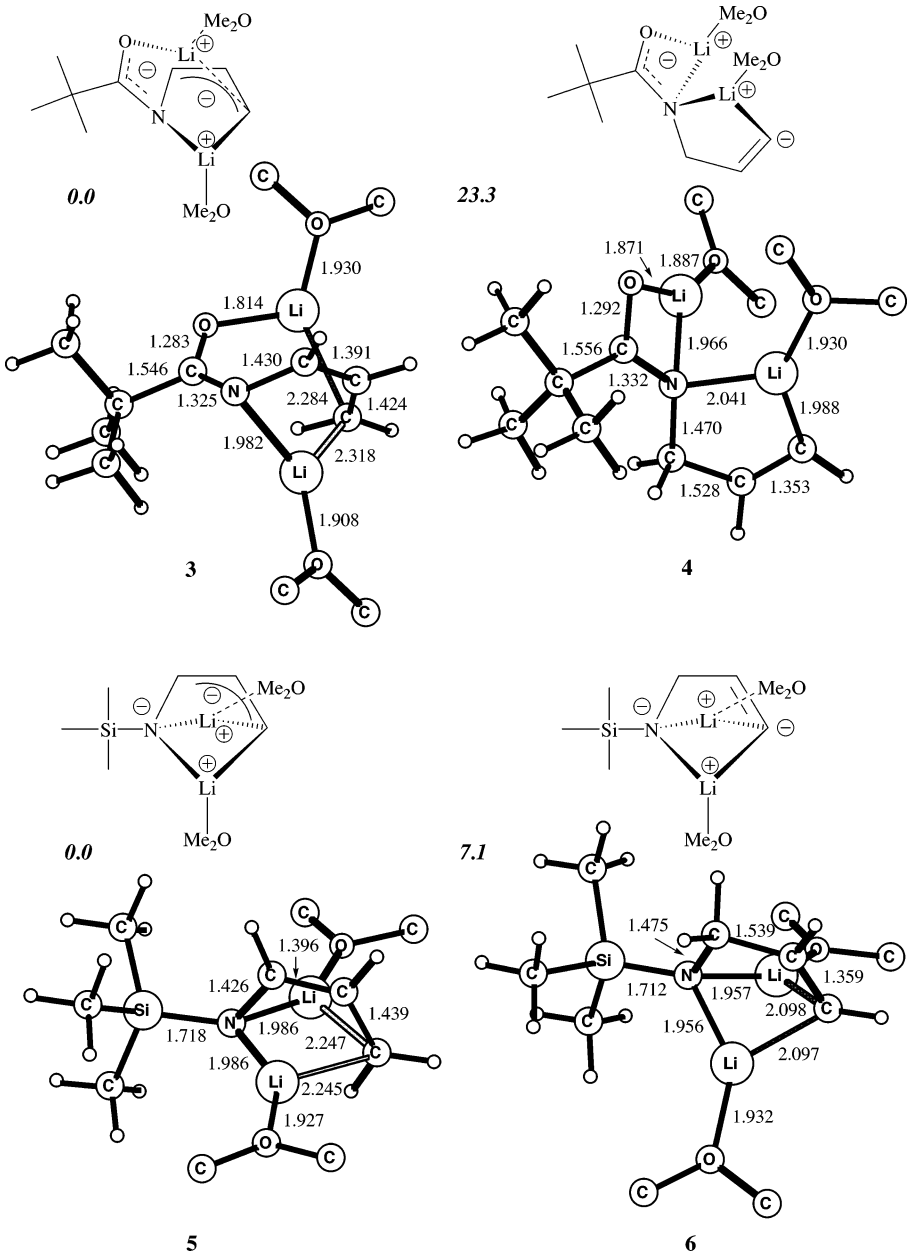

Figure 3. B3LYP/6-31+G* geometry-optimized structures of the *cis*-vinylic (**4**, **6**) and allylic (**3**, **5**) dianions. Selected bond lengths are given in angströms. Relative energies in kcal/mol are presented in bold italics.

the vinylic and the allylic dianion is 8 kcal/mol, favoring the lithiated allyl dianion.[7]

In this work, we present and interpret our results of the density functional theory (DFT) calculations. On the basis of these results, we suggest mechanisms for the deprotonation of **1** and **2**. We propose that the unexpected regioselectivity of the lithiation of **2** is under kinetic control.

Results from calculations on both the lithiated *cis*-vinylic and the allylic c-clamp-shaped dianions of **1** and **2** are presented first. The relative thermodynamic stability of these product structures will be discussed. We will also present and discuss more extensive calculations we performed to understand the kinetics of these reactions.

Results and Discussion

Relative Stability of the *cis*-Vinylic and Allylic Dianions of 1 and 2. The geometry-optimized structures of the dianions **3**−**6** are presented in Figure 3. Each of these four dianions was solvated with two molecules of dimethyl ether (Me_2O). The allylic isomers **3** and **5** are favored by 23.3 kcal/mol for the allylamide and 7.1 kcal/mol for the allylamine. The greater stability of allylic dianions **3** and **5** is not surprising considering that allylic anions are generally more stable than vinylic ones due to resonance stabilization of the negative charge. The bond lengths of the structures deprotonated at the allylic position clearly show strong delocalization with almost equal bond lengths (1.396 and 1.439 Å for the allylamine and 1.391 and 1.424 Å for the allylamide) (Figure 3). However, allylic delocalization of the carbanion in **5** places negative charge next to the negatively charged lithium-amide nitrogen. This effect is greatly reduced in **3** because most of the negative charge in the acylamide system is borne by the more electronegative oxygen atom. This explains the much greater difference between

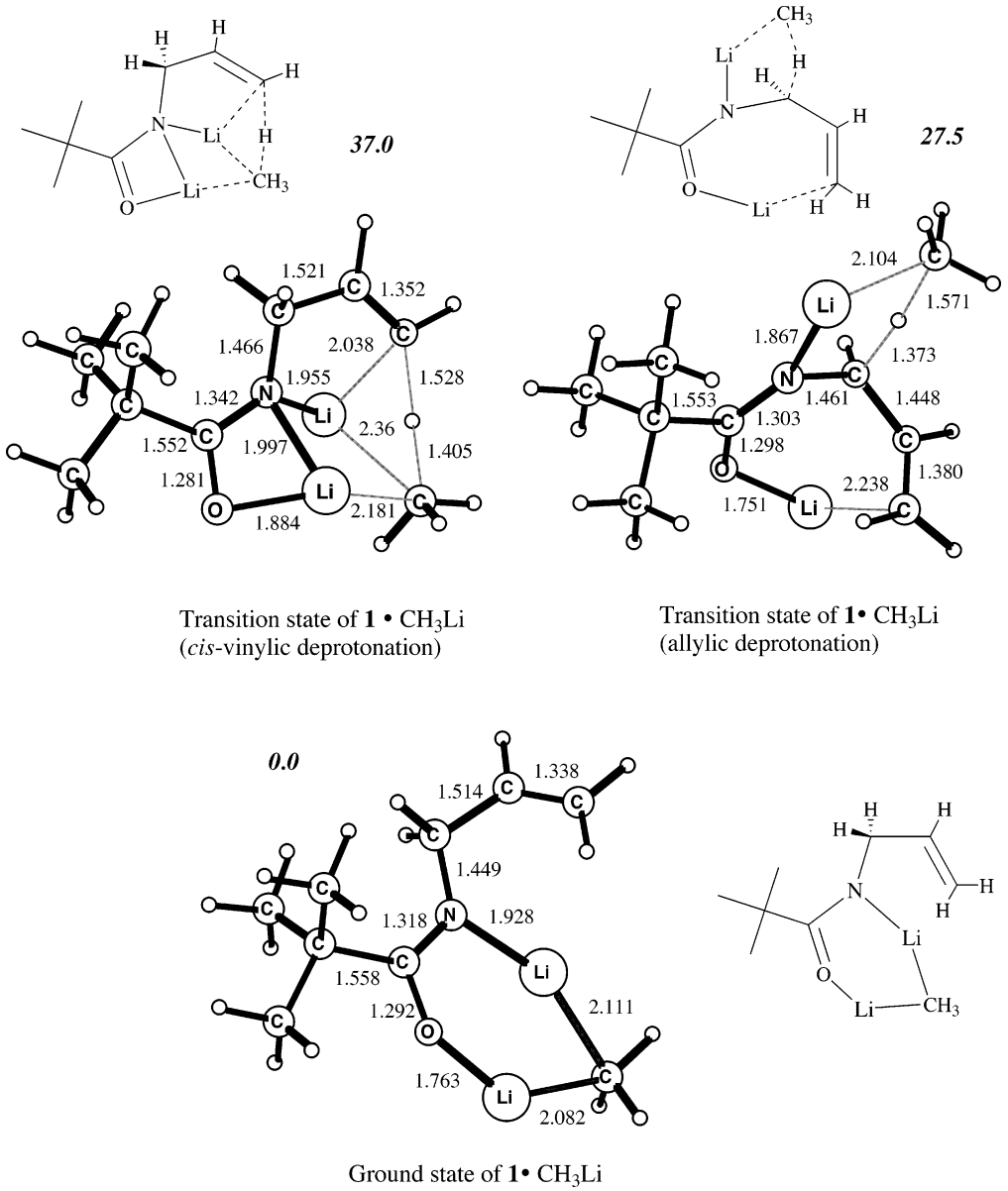

Figure 4. B3LYP/6-31+G* geometry-optimized structures of the gas-phase ground state and transition structures of the allylic and *cis*-vinylic deprotonations of **1**. Selected bond lengths are given in angströms. Relative energies in kcal/mol are presented in bold italics.

3 and **4** (23.3 kcal/mol) as compared to the difference between **5** and **6** (7.1 kcal/mol) The strong preference for allylic deprotonation of the allylamide can be understood from the efficient delocalization of the negative charge over the allyl anion.

From these calculations, it is clear that the observed *cis*-vinylic deprotonation of the allylamine cannot be under thermodynamic control. Consequently, the kinetics must be the controlling factor in this reaction. Hence, computations performed on the kinetics of the allyl amide deprotonation and the contrasting vinylic deprotonation for the allylamine are discussed next.

Kinetics of Deprotonation of *N*-Lithio-*N*-(*tert*-butyl)allylamide 1 in the Gas Phase with Explicit Ethereal Solvation Using B3LYP/6-31+G*. First, we present and discuss the energies and structures of the located and optimized stationary point geometries of **1**. Subsequently, deprotonation of **2** is described. In all cases, methyllithium (MeLi) is utilized in the computations to model the ^{n}BuLi because the smaller size is more appropriate for quantum chemical calculations. For similar reasons, THF solvation is modeled by Me_2O. Hydrocarbon solvent was simply represented by vacuum.

Deprotonation of *N*-Lithio-*N*-(*tert*-butyl)allylamide 1 in the Gas Phase. The ground state of **1**, shown in Figure 4 (bottom structure), was located, and its geometry was optimized using B3LYP/6-31+G*. Because the amide oxygen is more electronegative than the nitrogen, it strongly coordinates one of the lithium ions with a O−Li$^+$ bond length of only 1.763 Å. The other lithium ion coordinates to the deprotonated nitrogen with a bond length of 1.928 Å. The short amide C−N bond length (1.318 Å) indicates that it is mainly of double bond character. The corresponding amide C−O bond is long (1.292 Å), and, clearly, the negative charge resulting from amide deprotonation is mostly located on the oxygen. From this ground state, two transition state structures were located and geometry optimized. The top left structure in Figure 4 shows the transition structure of the *cis*-vinylic deprotonation. The *cis*-vinylic proton is partly

Table 1. Energies for the Deprotonation of Compounds **1** and **2**[a]

compound	TS, no solvent	TS, 2 Me_2O	product, 2 Me_2O
1 allylic	27.5	23.1[b]	−14.1[b]
1 *cis*-vinylic	37.0	31.8[b]	10.5[b]
2 allylic	31.4	29.6	−9.0
2 *cis*-vinylic	24.9	24.3	−1.4

[a] Energies are in kcal/mol and are relative the ground states. Zero-point energies are included. [b] Frequency calculations on the geometry-optimized structures of disolvated **1** were computationally out of reach. Zero-point energies computed for a smaller model of **1**, where the *tert*-butyl group was replaced by a hydrogen atom, were used instead.

transferred to the methyl anion with a bond distance of 1.528 Å to the vinylic carbon and with a distance of 1.405 Å to the methyl anion. The nitrogen now coordinates to both lithium ions. Only very small changes of the allyl carbon−carbon bond lengths have occurred from the ground state to the transition state. The calculated activation barrier for this deprotonation is 37.0 kcal/mol (Table 1), indicating a very slow reaction.

The corresponding transition structure for the allylic deprotonation is shown as the top right structure of Figure 4. The most obvious difference between the *cis*-vinylic and allylic deprotonation transition structures is that no C−Li bond rupture is necessary in the case of *cis*-vinylic deprotonation. Conversely, for allylic deprotonation, the bond between the methyl anion and one of the lithium cations is broken. At the transition state, the allylic proton has a bond distance of 1.373 Å to the allylic carbon, and the distance to the methyl anion carbon is 1.571 Å. The allylic carbon−carbon bond lengths change dramatically from 1.514 and 1.338 Å in the ground state to 1.448 and 1.380 Å at the transition state, indicating that the negative charge building up during the proton abstraction is efficiently delocalized over a forming allyl anion. The activation barrier was computed at 27.5 kcal/mol (Table 1). This deprotonation is 9.5 kcal/mol more favorable as compared to the *cis*-vinylic deprotonation. We are pleased to note that, experimentally, allylic deprotonation is exclusively observed in agreement with the computational results.[6]

Deprotonation of *N*-Lithio-*N*-(*tert*-butyl)allylamide 1 in THF Solvent with Explicit Ethereal Solvation. Experimentally, the deprotonation of **1** was carried out in THF solvent, and consequently this should be accounted for in the calculations. To model the THF solvent, 2 molecules of Me_2O were coordinated to the ground state and transition state structures previously geometry optimized in the gas phase. These structures were now reoptimized to the corresponding micro-solvated ground state and the transition state structures (Figure 5).

Only small structural changes occurred during the reoptimization of the solvated ground state where both lithium ions are coordinated by three ligands (the methyl anion, the amide oxygen or nitrogen, and one Me_2O molecule in a trigonal planar arrangement). The transition structure leading to *cis*-vinylic deprotonation is shown as the top left structure in Figure 5. The transition structure leading to allylic deprotonation is depicted as the top right structure. The structural changes going from the gas phase to the solvated transition structures are also small. The computed activation barriers are 23.1 kcal/mol (allylic) and 31.8 kcal/mol (*cis*-vinylic) (Table 1). We do not know how many THF molecules bind to **1** in the ground state; however, our calculations show that the relative rate of deprotonation at the allylic and the *cis*-vinylic positions is only dependent on the solvation to a small degree (9.5 kcal/mol allylic preference in the gas phase and 8.7 kcal/mol allylic preference in Me_2O micro-solvation). Further solvation of these complexes may reduce the activation barrier somewhat.

The Kinetics of Deprotonation of the Lithiated Allylamine 2 Investigated in the Gas Phase with Explicit Ethereal Solvation Using B3LYP/6-31+G*. A ground state of the mixed aggregate consisting of the lithiated *N*-(trimethylsilyl)allylamine **2** and one molecule of MeLi was geometry optimized, and its structure is presented as the bottom structure in Figure 6. Each lithium coordinates both to the negatively charged nitrogen and to the methyl anion. Inspection of these structures suggests that *cis*-vinylic and not *trans*-vinylic deprotonation should occur. *Cis*-vinylic deprotonation is observed experimentally. From this structure, we searched for a transition structure in which the *cis*-vinylic proton is abstracted by the methyl anion. At the transition state, the proton is 1.476 Å from the vinylic carbon and 1.452 Å away from the methyl anion (top left structure in Figure 6). The carbon−carbon bond lengths of the allyl moiety change only slightly from those of the ground state. The C2−C3 double bond stretches from 1.340 Å in the ground state to 1.354 Å at the transition state, and the C1−C2 single carbon bond stretches from 1.508 to 1.520 Å (Figure 6).

The significant difference lies in the coordination of the vinylic carbon in the ground state and at the transition state. In the ground state, the vinylic carbon is not in contact with any of the lithium ions. However, at the transition state, where it is partly negatively charged, it coordinates to both lithium ions with distances of 2.243 and 2.231 Å. It seems likely that the electrostatic interaction between the forming carbanion and the lithium ions stabilizes the transition structure and helps lower the activation barrier. The activation barrier was computed to 24.9 kcal/mol (Table 1). The transition structure leading to allylic deprotonation is presented in Figure 6 (top right structure). The *cis*-vinylic and the allylic transition state structures differ in their aggregation states. This is also observed in the case of the amide deprotonation. While the *cis*-vinylic deprotonation occurs with no change in aggregation, the allylic deprotonation can only occur when the methyl anion breaks its bond to one of the lithium ions, as shown in Figure 6. Consequently, for deprotonation at the allylic position to occur, the methyl anion must first break its bond to the lithium cation, then swing around and come in proximity to one of the allylic protons. The transition state occurs when the proton is transferred 1.335 Å from the allylic carbon and 1.602 Å from the methyl anion carbon. Surprisingly, this activation barrier was computed to be 6.5 kcal/mol higher in energy than that of the *cis*-vinylic transition structure. We suggest that this odd preference for *cis*-vinylic deprotonation is due to the negative charge on the neighboring nitrogen. Due to the close proximity of the methyl anion to the *cis*-vinylic proton, an alternative explanation for the *cis*-vinylic deprotonation could be the principle of least motion.

Unlike the acylamide monoanion, the negative charge in the secondary amide monoanion **2** is completely localized on the nitrogen. Hence, when the allylic proton is being pulled off by the methyl anion, negative charge starts to build up on the allylic carbon, which causes an energetically unfavorable charge−charge repulsion between the developing negative charge on the allyl carbon and the negatively charged nitrogen. The allyl carbon is sp^3-hybridized in the ground state, and after proton

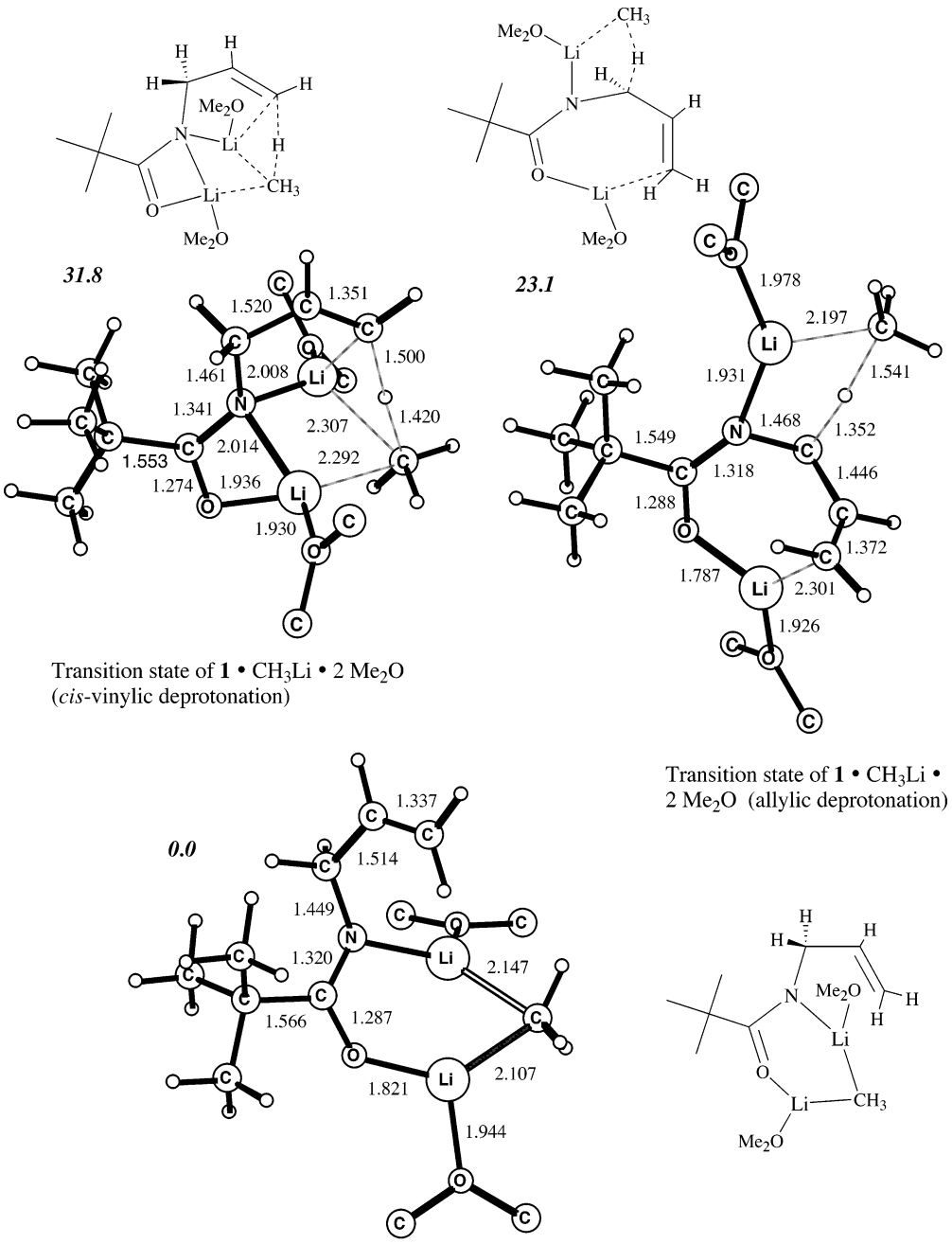

Figure 5. B3LYP/6-31+G* geometry-optimized structures of the micro-solvated (2 molecules of Me_2O) ground state and transition structures of the allylic and *cis*-vinylic deprotonations of **1**. Selected bond lengths are given in angströms. Relative energies in kcal/mol are presented in bold italics.

transfer to the methyl anion is completed, it is sp^2-hybridized. At the transition state, it is a mixture of the two and efficient charge-delocalization through resonance has not yet fully developed. The carbon−carbon bond between the allyl carbon and its neighboring carbon is 1.508 Å in the ground state (Figure 6), which indicates that it is a single bond. At the transition state, it has shortened to 1.462 Å (Figure 6), and, finally, in the deprotonated product as depicted in Figure 3 (bottom left structure), it has shortened to 1.396 Å. This last value indicates that the carbon−carbon bond is now part of an allyl anion with fully developed resonance.

Partial charges were derived (see Computational Details) for the ground state and the *cis*-vinylic and allylic transition state structures of **2**, see Figure 6. The partial charge on C1 in the ground state is 0.65. At the *cis*-vinylic transition state, this charge has decreased to 0.48, and for the allylic deprotonation it has decreased to 0.23. The partial charge on the nitrogen is −1.28 in the ground state, and it changes only little up to both transition states. The partial charges on the C2 and C3 carbons change from −0.17 and −0.37 in the ground state to −0.12 (*cis*-vinylic and allylic), −0.61 (*cis*-vinylic), and −0.58 (allylic) at the transition states. The large negative charge on the C3 carbon at both transition states is only efficiently stabilized in the *cis*-vinylic deprotonation where both lithium ions help in stabilizing the negative charge developing on the C3 carbon. At the allylic transition state, one lithium cation stabilizes the nega-

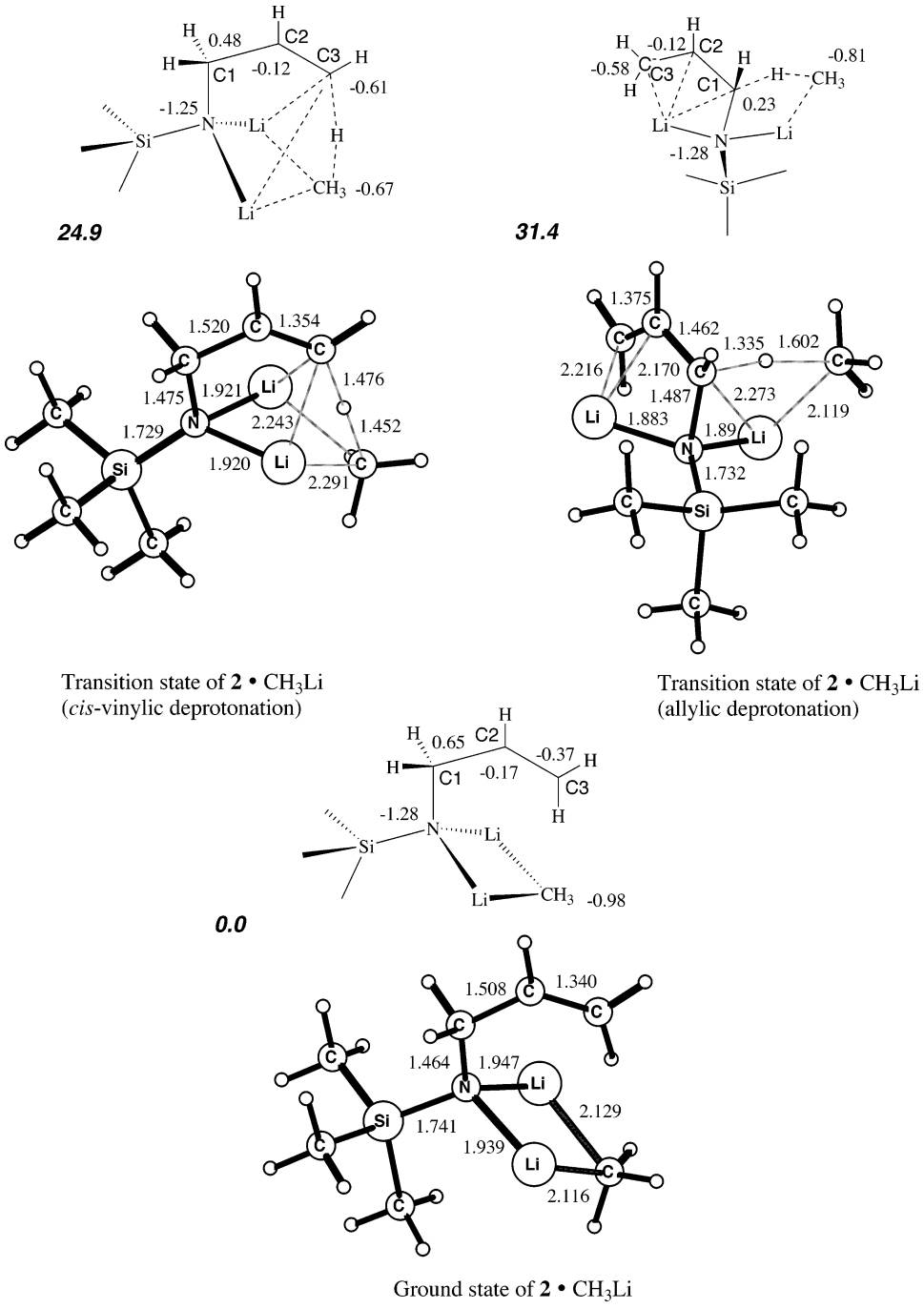

Figure 6. B3LYP/6-31+G* geometry-optimized structures of the gas-phase ground state and transition structures of the allylic and *cis*-vinylic deprotonations of **2**. Selected partial charges are presented in the schematic figures over each structure. Relative energies in kcal/mol are presented in bold italics.

tive charge developing on the C3 carbon, while the other lithium ion helps to stabilize the proton transfer located at the C1 carbon.

The lithium ions in the mixed aggregate, formed between **2** and BuLi, are solvated by two molecules of THF as determined by us by NMR.[6] Thus, we decided to investigate the role of solvation on the activation barriers of deprotonation by micro-solvating the ground state and transition state geometries of **2** with two molecules of Me_2O. The reoptimized ground state and transition state geometries, solvated with two Me_2O molecules, are presented in Figure 7. The computed activation barrier to *cis*-vinylic deprotonation is 24.3 kcal/mol, only slightly lower than that of the gas-phase reaction (Table 1). The corresponding micro-solvated allylic deprotonation was computed to be 1.8 kcal/mol more stable than the nonsolvated, gas-phase reaction. However, *cis*-vinylic deprotonation is still favored by 5.3 kcal/mol. The calculations suggest that there is only a slight difference in reactivity of the mixed aggregate in a hydrocarbon solvent (approximated here by vacuum) and THF solvent. The explanation as to why the deprotonation proceeds readily in THF, while no deprotonation occurs in a hydrocarbon solvent, may be that THF promotes the formation of the "c-clamp" aggregate, while the hydrocarbon solvent does not. The results of the calculations suggest that this aggregate is able to deprotonate both **1** and **2**. Consequently, the explanation to the rather surprising observation that deprotonation occurs in THF

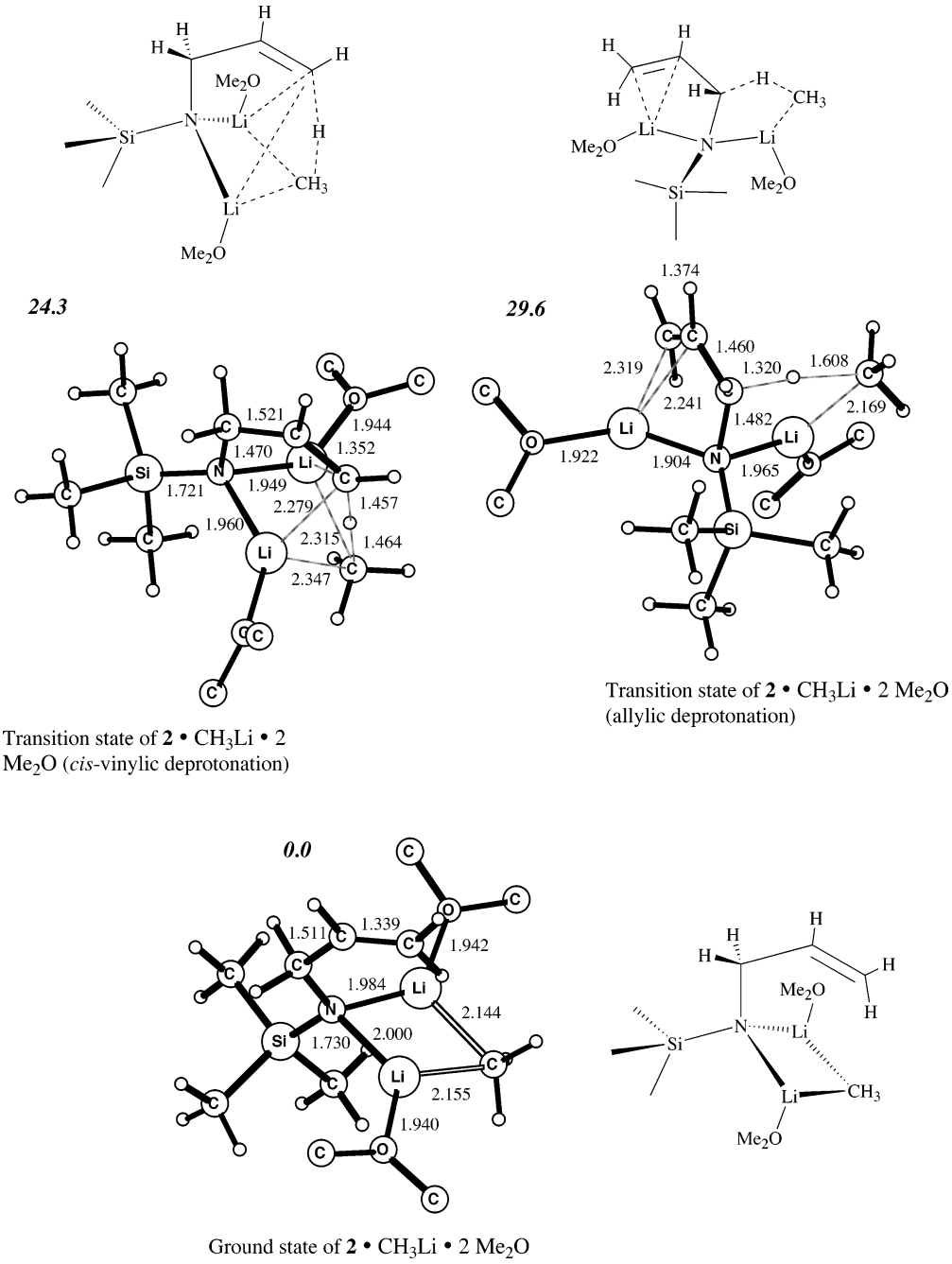

Figure 7. B3LYP/6-31+G* geometry-optimized structures of the micro-solvated (2 molecules of Me_2O) ground state and transition structures of the allylic and *cis*-vinylic deprotonations of **2**. Selected bond lengths are given in angströms. Relative energies in kcal/mol are presented in bold italics.

but not in a hydrocarbon solvent may lie in their different ability to aggregate the organolithiums.

Deprotonation of **1** and **2** was computed to be exothermic (Table 1). The *cis*-vinylic deprotonation of **2** was computed to be −1.4 kcal/mol exothermic, and the allylic deprotonation of **1** was computed to be downhill in energy by 14 kcal/mol. Due to the higher basicity of butyllithium as compared to that of methyllithium (used in the calculations), the reactions are expected to be more exothermic than the calculations indicate. Also, the increase in entropy when forming butane should increase the exothermicity of the reactions.

Conclusions

The DFT calculations demonstrate that deprotonation of the allylic proton of allylamine **2** will not occur, even though the corresponding deprotonated product is more thermodynamically stable than the deprotonated *cis*-vinylic isomer. Deprotonation of **2** is consequently kinetically controlled. Furthermore, both the computed activation barrier of allylic deprotonation of allylamide **1** and the energy of the deprotonated product are favored over the corresponding energies of the *cis*-vinylic deprotonation. The computational results of this study agree with experimental observations.

Computational Details

Geometry optimization of all structures was conducted using the B3LYP nonlocal gradient-corrected functional and the split-valence 6-31+G* basis set. Frequency calculations were performed on all of the optimized structures using the same level of theory. Ground state

and product geometries were found to have real frequencies, while the transition state geometries contain one imaginary frequency each. Zero-point energies were computed using the nonscaled harmonic frequencies. Partial charges for the ground state and the transition structures of the *cis*-vinylic and allylic deprotonation of **2** were derived using B3LYP/6-31+G* and the CHelpG scheme (which adjusts the partial charges to fit the computed electrostatic potential) as implemented in Gaussian 98. All calculations were performed using the Gaussian 98 program.[8]

Acknowledgment. This work was supported by PHS Grant GM-35982 and NSF Grant 0213381.

Supporting Information Available: Geometry-optimized structures and energies of the stationary points. This material is available free of charge via the Internet at http://pubs.acs.org.

JA0487731

(8) Frisch, M. J.; Trucks, G. W.; Schlegel, H. B.; Scuseria, G. E.; Robb, M. A.; Cheeseman, J. R.; Zakrzewski, V. G.; Montgomery, J. A., Jr.; Stratmann, R. E.; Burant, J. C.; Dapprich, S.; Millam, J. M.; Daniels, A. D.; Kudin, K. N.; Strain, M. C.; Farkas, O.; Tomasi, J.; Barone, V.; Cossi, M.; Cammi, R.; Mennucci, B.; Pomelli, C.; Adamo, C.; Clifford, S.; Ochterski, J.; Petersson, G. A.; Ayala, P. Y.; Cui, Q.; Morokuma, K.; Malick, D. K.; Rabuck, A. D.; Raghavachari, K.; Foresman, J. B.; Cioslowski, J.; Ortiz, J. V.; Baboul, A. G.; Stefanov, B. B.; Liu, G.; Liashenko, A.; Piskorz, P.; Komaromi, I.; Gomperts, R.; Martin, R. L.; Fox, D. J.; Keith, T.; Al-Laham, M. A.; Peng, C. Y.; Nanayakkara, A.; Gonzalez, C.; Challacombe, M.; Gill, P. M. W.; Johnson, B.; Chen, W.; Wong, M. W.; Andres, J. L.; Gonzalez, C.; Head-Gordon, M.; Replogle, E. S.; Pople, J. A. *Gaussian 98*, revision A.7; Gaussian, Inc.: Pittsburgh, PA, 1998.